JOURNAL OF MATERIALS SCIENCE **40** (2005) 373–380

Evaluation of the electrical potential drop technique in the determination of crack growth resistance-curves of Carbon/Carbon composites and carbon bonded refractories

A. ANTONARULRAJAH, V. P. S. RAMOS, S. B. FAZLUDDIN, B. RAND
Institute for Materials Research, School of Process, Environmental and Materials Engineering, University of Leeds, Leeds LS2 9JT, UK
E-mail: materials@leeds.ac.uk

Electrical potential drop (EPD) and compliance techniques are compared as techniques for crack length measurement in determining the crack growth resistance-curve (*R*-curve) of two Carbon/Carbon (C/C) composites and two carbon-bonded oxide-graphite refractories. The two C/C composites differ in the strength of the fibre/matrix interaction, resulting from the use of untreated and surface treated carbon fibres. The refractories differ in the volume fraction of graphite flakes. *R*-curve measurements on the C/C composites were made on specimens with chevron notches whilst straight-through notches were used for carbon bonded refractories. In the EPD method, the instantaneous crack length was determined from the instantaneous electrical potential across the notch plane, which was recorded in line with load and displacement data, and experimental calibration data. In the compliance method, the instantaneous crack length was determined analytically using the instantaneous load and displacement data. From the EPD technique smaller crack lengths were calculated than from the compliance technique in the regions of fracture where the composites had well developed process zones, and for the whole region in the refractories. The EPD technique underestimates the actual crack length, due to current conduction in the wake zone by bridging fibres/grains, and as a result the *R*-curves are different from those reported by the compliance technique, which are considered to be more reliable. The compliance-based results are used to establish the effects of fibre surface functionality and graphite flake content on crack growth resistance in the two systems.

1. Introduction

The *R*-curve describes the resistance of a material against any crack growth. It can be described by the stress intensity factor (K_1) as a function of the crack length during its growth [1]. The precise determination of the *R*-curve of a material requires that the lengths of growing cracks be measured accurately. The major problem in measuring the crack length in toughened ceramics and composites is the uncertainty in defining the crack-front, because of the large process zone which occurs due to extensive crack branching.

A conventional method of crack length measurement is the use of a travelling optical microscope, to directly measure the crack length. A high-speed camera is incorporated with it for faster recording of crack lengths. Although this technique had been used in several studies on various materials [1–3], it is not suitable for materials which show extensive crack branching. For example, note the fracture surfaces of the Carbon/Carbon (C/C) composite given in Fig. 1. The difficulty in using the optical technique in these composites is that the crack front is not well defined or confined to the notch plane. The crack length detected from the free surface, around the notch tip where the microscope is focused, may not represent the overall crack on the notch plane. The inapplicability of microscopy to a chevron-notched specimen, where the crack tip is inside the specimen, is another limitation.

The other major techniques which are recommended or used to determine crack lengths indirectly are the compliance [4–6] and Electrical Potential Drop (EPD) [7–12] techniques. The compliance method is based on the concept that the stiffness of a body decreases with crack growth [13]. The EPD is based on the concept that the electrical field in a cracked specimen with a current flowing through it is a function of the specimen geometry, and in particular the crack area. For a constant current flow, the electrical potential across the crack plane increases with increasing crack size due to modification of the electric field. The change in voltage can be related to crack size through analytical or experimental calibration relationships [11]. In principle

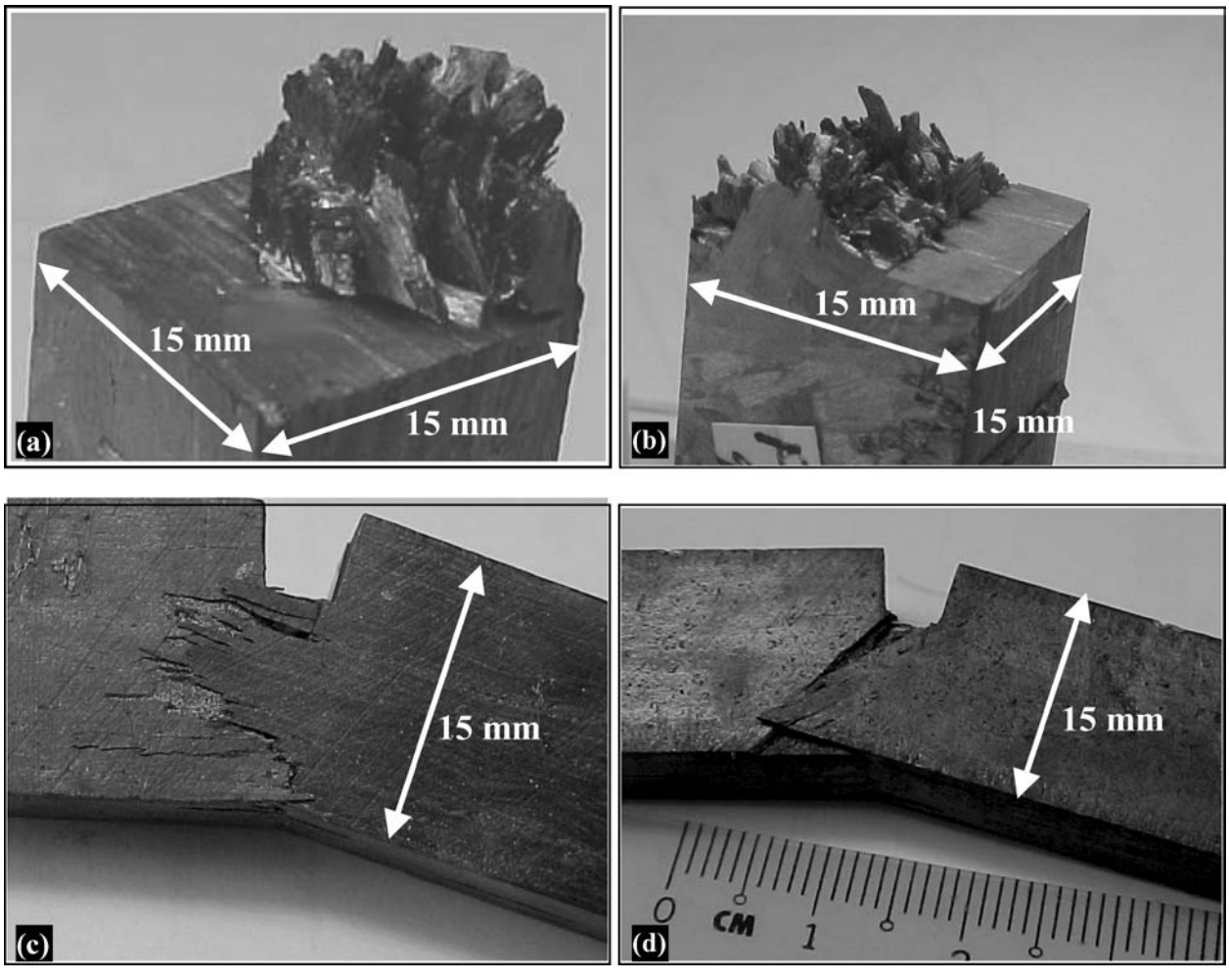

Figure 1 Digital camera images of partly and completely fractured specimens of Carbon/Carbon composites showing the complexity of the crack front: (a) chevron-notched specimen, (b) straight-through notched specimen, (c) straight-through notched specimen of commercial Aircraft brake component, and (d) the opposite side of specimen '(c)'.

this method seems to offer advantages in that the whole crack area can be monitored. This study investigates the applicability of the EPD technique with experimental calibration for measuring the crack length in C/C composites and carbon bonded graphitic refractories. The EPD technique is compared with the compliance technique as a means of crack length measurement. The crack lengths are then used to construct *R*-curves.

2. Experimental procedure

2.1. Materials

2.1.1. Carbon/Carbon composites

Two discontinuous-fibre C/C composites were examined, fabricated by a filament winding and hot press moulding technique. The fibre length was in a range from 5 to 7 mm, and the volume fraction of fibres in the composite was about 65 to 68%. One composite contained P100 carbon fibres and the other contained P55S. P100 is a non surface-treated fibre and P55S is a surface-treated fibre, and both are mesophase pitch based, supplied by Amoco Inc. (now Cytec Industries Inc.), USA. The carbon matrix was built up from phenolic resin, which was supplied by Borden Chemicals UK Ltd. The rationale behind the selection of these two commercial carbon fibres was to characterise the *R*-curve behavior of C/C composites with different fibre/matrix interaction. A filament winding rig was used to soak the continuous carbon fibre-tow in phenolic resin, followed by chopping the soaked tows and hot pressing to mould a composite disc of 100 mm in diameter and about 10 mm in thickness. The temperature and pressure of pressing was 200°C and 6 MPa. Mechanical test samples were cut from the disc, carbonised at 1000°C. The samples were then densified by multiple impregnations with the same phenolic resin and carbonisation at 1000°C. Fig. 2 shows that in the composite of the untreated fibre (P100) the matrix shrinks away from the fibres leaving voids at the fibre/matrix interface, and therefore this composite is said to have weak fibre/matrix interaction. On the other hand, the matrix adheres well to the surface-treated fibre (P55S) and accommodates the voids within the matrix. The voids originate from the significant volumetric shrinkage of the matrix that occurs during carbonisation. Thus, this latter composite possesses strong fibre/matrix interaction. Some physical and mechanical properties of the composites are given in Table I.

2.1.2. Carbon-bonded refractories

The Alumina-Carbon refractories that are studied here find application mainly in steel making industries [14]. The refractories are produced by axial pressing of

TABLE I Some physical and mechanical properties of the composites and refractories

	P100	P55S	4% Graphite	8% Graphite
Bulk density (kgm^{-3})	1760	1630	3040	3020
Open porosity (%)	11	10	16.0	14.4
Flexural modulus (GPa)	24	28	20.8	14.1
Flexural strength (MPa)	91	112	27.9	20.0

a mixture containing fused alumina, metallic silicon, graphite flake and Novolac phenolic resin. The fused alumina comprised a wide particle size distribution varying from sub-micron powder to large polycrystalline particles, or grains, of size 1.7 mm. Two refractories were used in this study, containing 4 and 8% graphite. Both were produced using the same particle size distribution, calculated using the Andreasen model with the distribution modulus of $n = 0.4$ [15] to give a high packing density. After curing the resin binder (110°C for 24 h plus 250°C for 12 h) the bricks were heat-treated at 1350°C for 5 h, under a reducing atmosphere, embedded in a graphite bed, inside a ceramic container. As a result, a silicon carbide bond phase is formed by the reaction between the metallic silicon and carbon [16]. This reaction did not go to completion and some un-reacted silicon is present as shown in the micrograph in Fig. 3. The material comprises the polycrystalline alumina grains, graphite flakes, un-reacted silicon and a silicon carbide and carbon bond. The large polycrystalline alumina grains are fairly closely packed with the interstices filled by the finer particles and bonding materials. Table I shows some physical and mechanical properties of these refractories along with those of the C/C composites.

2.2. Specimen preparation and mechanical testing

For the C/C composites, bar samples of square cross section of about 10 mm × 10 mm × 60 mm were cut from the composite discs then carbonised, impregnated with the same resin and re-carbonised to fill the pores generated during carbonisation. The re-impregnation and re-carbonisation continued for four further cycles. Then, a chevron notch was machined using a 200-μm thick diamond impregnated cutting wheel, while the specimen was seated on a specially designed jig to produce a chevron notch-tip angle of 80° as recommended by the ASTM standard C1421-99 [17] for three-point bend specimens. For refractories, samples of square cross section of about 20 mm × 20 mm × 100 mm were cut from original bricks and a 'straight-through' notch was cut. All samples were tested under three point bending on a Mayes mechanical testing machine with

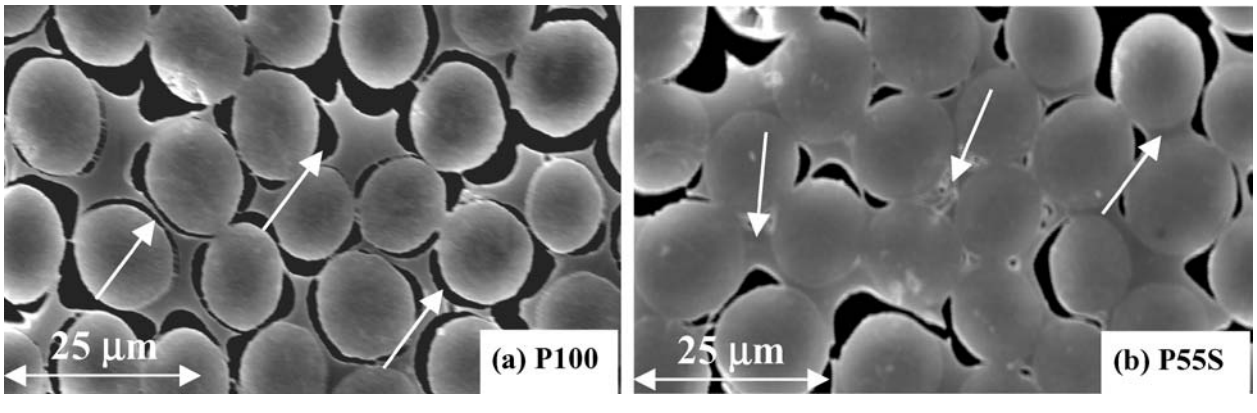

Figure 2 SEM images of C/C composites showing different fibre/matrix interactions: (a) P100, where arrows show weak fibre/matrix interaction and the voids are mainly located at the fibre/matrix interface. (b) P55S, where arrows show strong fibre/matrix interaction and the voids in this composite are present within the matrix.

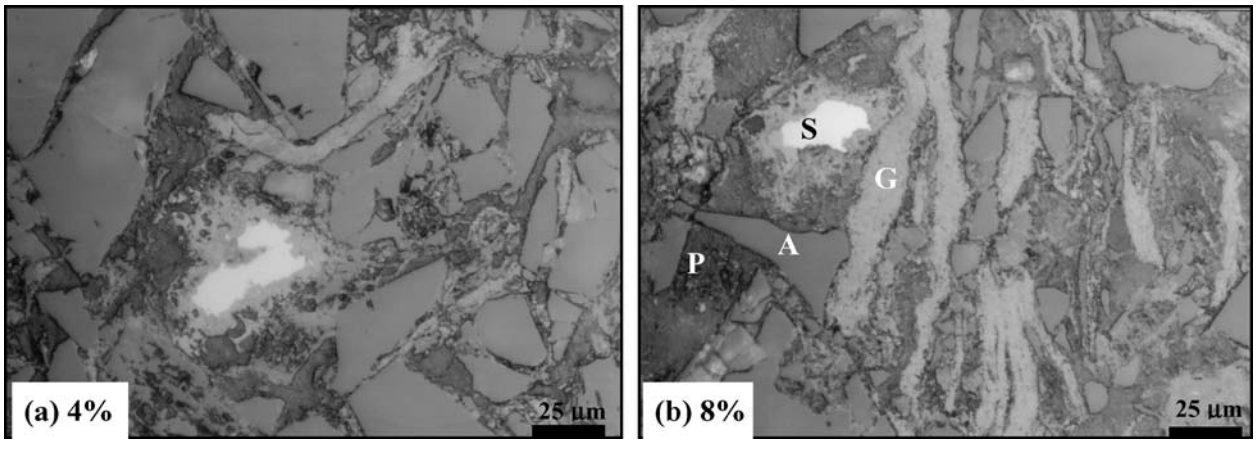

Figure 3 Optical photomicrography of the refractory composite with (a) 4% graphite and (b) 8% graphite. Obs.: A = fused alumina; G = graphite flake; S = unreacted silicon; P = porosity.

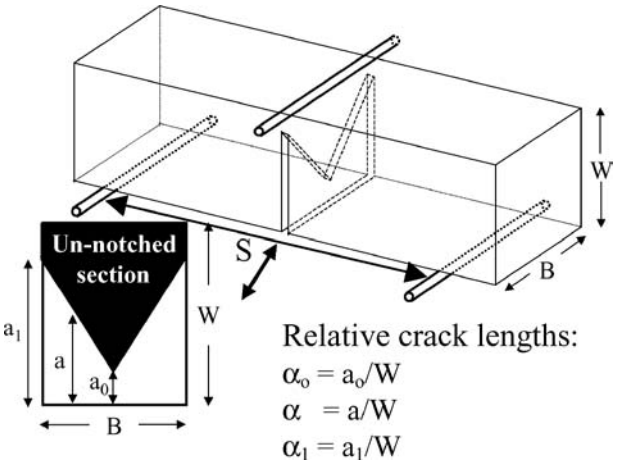

Figure 4 Geometry and nomenclature of the chevron-notched three-point bend specimen.

a 5 kN load cell. The tests were carried out under displacement control with cross head speeds of 50 μm/min for composites and 5 μm/min for refractories, which would be slow enough to produce stable crack propagation. The loading span was 45 and 80 mm respectively. All testing involved the incorporation of EPD equipment to monitor the electrical resistance changes across the notch plane during the complete test. A constant direct current (DC) of 1 A was supplied at the two ends of the sample. Samples were electrically insulated from the loading-jig. The data of load (P) and EPD (V) versus displacement (D) were acquired by a direct computer link via an oscilloscope. Fig. 4 is a schematic representation of the chevron-notched specimen under three-point bending.

2.3. Crack length deduction techniques

2.3.1. Compliance technique

The change in compliance (C) of a specimen due to crack propagation can be used to establish the crack length. The instantaneous compliance at any point during a stable fracture can be used to determine the crack length at that point. The theoretical change in compliance with crack propagation, $\frac{dC}{d\alpha}$, can be related to the stress intensity factor at the crack tip (K_1), load on the sample (P), Young's modulus (E) of the sample, and the sample thickness (B) according to Equation 1 [4, 13, 18].

$$\frac{dC}{d\alpha} = \frac{2K_1^2 B}{P^2 E} \tag{1}$$

where K_1, for a three-point bend straight-through notched bar specimen, is given as

$$K_1 = \frac{PS}{BW^{1.5}} Y(\alpha) \tag{2}$$

and K_1, for a three-point bend chevron notched bar specimen, is given as

$$K_1 = \frac{PS}{BW^{1.5}} Y(\alpha) \left(\frac{\alpha_1 - \alpha_o}{\alpha - \alpha_o}\right)^{0.5} \tag{3}$$

and,

$$Y(\alpha) = \left(\frac{3\alpha^{0.5}(1.99 - \alpha(1-\alpha)(2.15 - 3.93\alpha + 2.7\alpha^2))}{2(1+2\alpha)(1-\alpha)^{1.5}}\right) \tag{4}$$

The parameters α_o, α, α_1, B, W, S for a chevron-notched three-point bend specimen are defined in Fig. 4. P is the instantaneous load.

For straight-through notched specimens, substituting Equation 2 into 1, and then integrating gives:

$$\int_{C_{\alpha_0}}^{C_\alpha} dC = C(\alpha) - C(\alpha_o) = \frac{2S^2}{BEW^3} \int_{\alpha_0}^{\alpha} Y^2(\alpha)\, d\alpha \tag{5}$$

Similarly, for chevron-notched specimens, substituting Equation 3 into 1, and then integrating gives:

$$\int_{C_{\alpha_0}}^{C_\alpha} dC = C(\alpha) - C(\alpha_o) = \frac{2S^2(\alpha_1 - \alpha_0)}{BEW^3} \int_{\alpha_0}^{\alpha} \frac{Y^2(\alpha)}{(\alpha - \alpha_0)} d\alpha \tag{6}$$

$C(\alpha)$ is the instantaneous compliance, which is the instantaneous displacement divided by the relevant load. $C(\alpha_o)$ is the compliance at the onset of cracking. The parameters $\alpha_o, \alpha_1, S, B, W$, and E are all known. The solution to integration, which was performed using Mathcad 2001, generates the instantaneous α (normalised crack length) for given instantaneous compliance. The load at which the load-displacement plot deviates from its (initial) linearity was chosen as the point of crack initiation.

2.3.2. Electrical potential drop technique

When a body is supplied with a constant current, the electrical resistance across two points/planes increases if the cross sectional area anywhere between those two points/planes decreases. Crack propagation during a fracture causes such a reduction in the cross sectional area along the notch plane. The increasing electrical resistance (or voltage) can be translated to crack length through experimental calibration. Fig. 5 shows one such experimental calibration curve of one of the C/C composites of this study. The instantaneous normalised crack length can be obtained from the calibration curve and the relevant voltage-displacement curve that will be obtained during mechanical testing (presented in Fig. 6).

2.4. Calculation of stress intensity factors

The R-curves are represented as the stress intensity factor (K_1) versus normalised crack length. Values of K_1 as a function of normalised crack length were calculated using Equation 2 for straight-through-notched specimens and using Equation 3 for chevron-notched specimens.

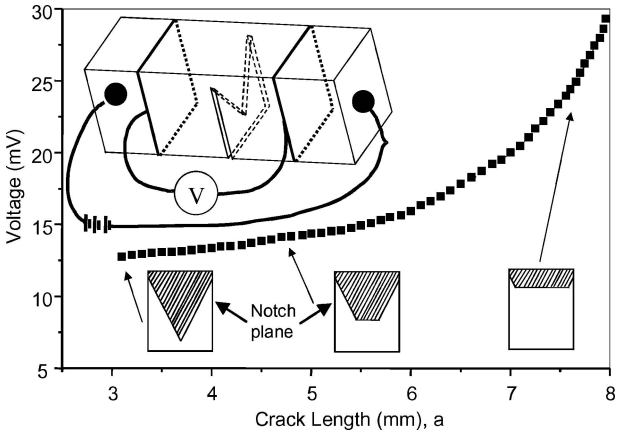

Figure 5 An experimental calibration curve (voltage across the notch plane versus crack length) of P100, showing also a schematic representation of the experimental set-up during its determination.

3. Results and discussions

3.1. Load & voltage versus displacement curves

C/C composites. The load-displacement curves, to a certain extent, characterise the different fracture behavior of the composites under flexure. In the P55S composite, the load dropped to zero and the test sample fractured totally (i.e., into two halves) at a displacement of about 1.5 mm. However, the P100 composite showed a higher resistance to fracture and continued to flex over 3 mm without separating. The strong interaction between the fibre and the matrix results in the of P55S composite displaying relatively poor resistance to fracture. The faster fracture occurs because the cracks do not distinguish the fibre/matrix interfaces, which do not debond. The P100 composite, on the other hand, shows higher resistance to fracture because of the weak fibre/matrix interfaces, deflect the crack from its original notch plane and allow a higher utilisation of the fibre strength. The different fracture behavior between the composites is also shown by their potential drop curves: a steep rise in the voltage of the P55S composite indicates the fast crack propagation, and a very gentle rise in that of the P100 composite indicates more gradual fracture behavior. The higher initial voltage of P55S across the notch plane, which is not relevant to the fracture behavior, occurs because of the higher electrical resistivity of P55S compared to P100.

Refractories. Unlike the composites, the two refractories show very similar fracture behavior as shown by their load—displacement plots which almost overlap one another, except that the refractory that contained 4% graphite is able to sustain a higher load. The flexural strengths are shown in Table I. Compared to the composites, the refractories are quite brittle, as fracture takes place at much lower displacement. The higher initial voltage across the notch plane in the refractory with 4% graphite is simply because it contained a smaller volume fraction of the conducting carbon constituents.

3.2. Normalised crack length versus displacement plots

The normalised crack lengths (a/W) are plotted in Fig. 7 as a function of the cross-head displacement. The curves, determined by the two techniques, are quite different for the same specimen. In the C/C composites the EPD technique results in shorter crack lengths than the compliance technique at low displacements, but the reverse is the case at higher displacements when the crack lengths are appreciable. This is highlighted in Fig. 8. It is noteworthy that the cross-over points occur at significantly different displacements for the P55S and P100-based composites, respectively at 0.32 and 0.54 mm. Again, for the two refractory materials different crack length—displacement curves are given by the two techniques. However, in this case the EPD technique always results in a shorter crack length than the compliance method at the same displacement and there is no cross-over point for these systems.

Fig. 9 shows the fracture surfaces for the various materials. In both C/C composites significant pull out of fibres and fibre tows is evident, this being very much more pronounced for the P100 fibre based composite in which the fibre-matrix bonding is weak. The fracture surfaces of the refractories are quite rough, showing evidence of transgranular fracture and of pull out of graphite flakes. Clearly, there must be significant bridging of the main crack in its wake during the crack propagation, by fibres in the case the C/C composites and by graphite flakes and carbon-coated alumina

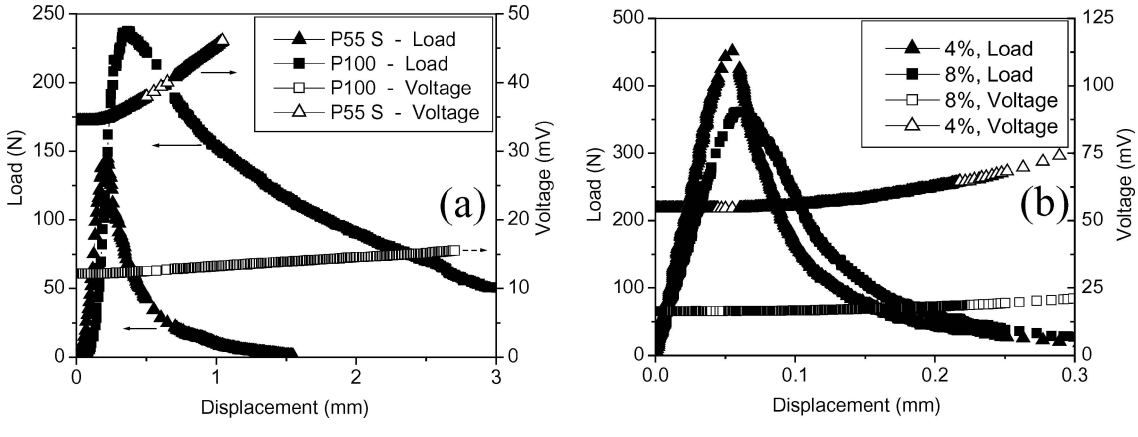

Figure 6 Load and voltage versus displacement plots of fracture testing: (a) C/C composites and (b) carbon-bonded refractories.

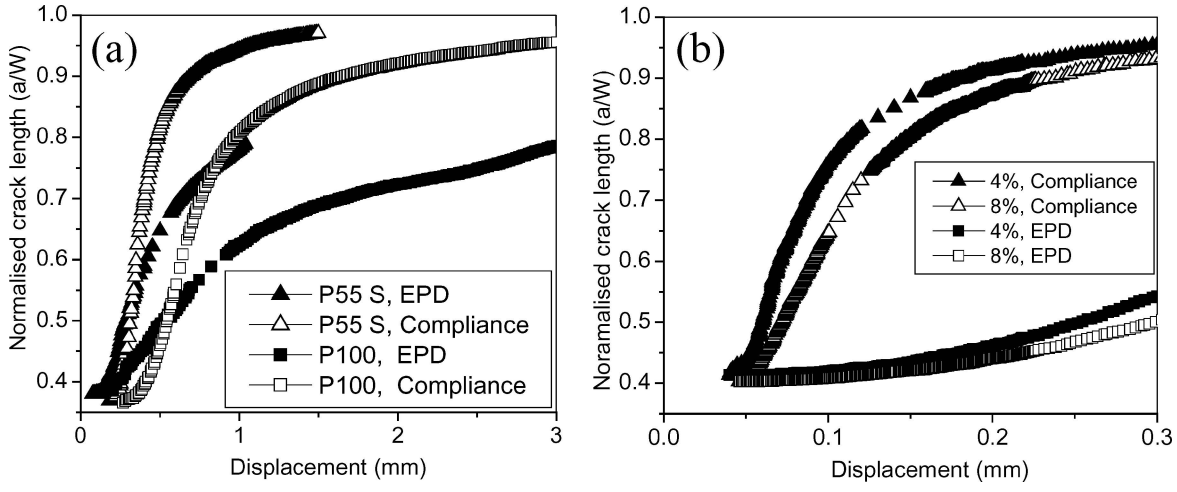

Figure 7 Normalised crack length versus displacement plots: (a) C/C composites and (b) carbon bonded refractories.

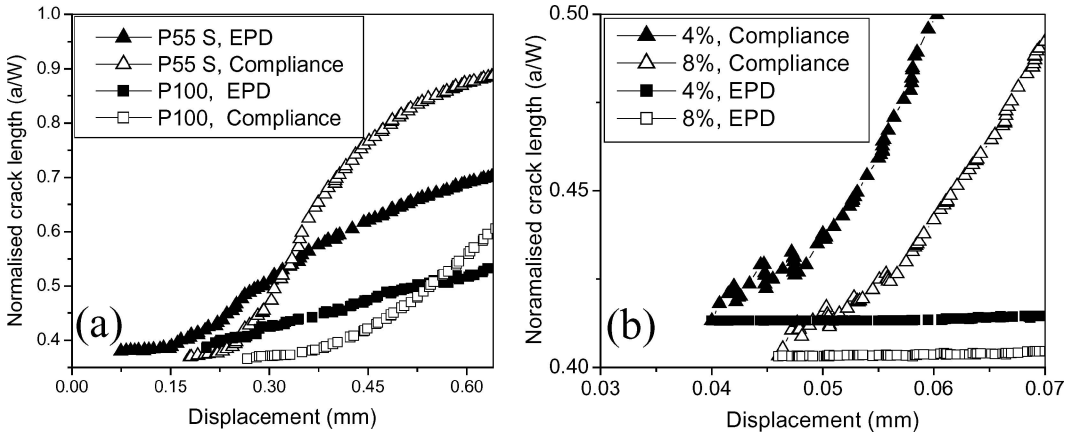

Figure 8 Initial trend (at small displacements) of Normalised crack length versus displacement plots of fracture testing: (a) C/C composites and (b) carbon-bonded refractories.

polycrystalline grains in the case of the refractories. These bridging components are electrically conducting and this will result in a reduced electrical resistivity leading to an underestimation of the crack length as deduced from the EPD calibration curve. This crack bridging effect is dominant for the refractories over the whole crack propagation process, but not so for the C/C composites.

Another effect, common in brittle matrix composites, is sub-critical cracking of the matrix. This is well-known to occur for C/C composites and is more predominant when the fibre-matrix interface is weak. This is most likely the origin of the overestimate of crack length at low displacement given by the EPD technique for these composites. Sub-critical cracking ahead of the main crack will increase the measured resistivity and appear in the analysis as a longer length of crack than actually exists. This does not affect the compliance analysis significantly because the stiffness is very greatly dominated by the fibres. Furthermore, the geometry of the chevron notch means that the cross-sectional area affected by the sub-critical cracking is large compared with that affected by the propagation of the main crack in the initial stages of propagation of that crack. This is not the case for the straight-through notch and this may be partly responsible for the refractory materials not displaying the same cross-over behavior.

3.3. *R*-curves

The *R*-curves of composites and refractories are presented in Fig. 10. Those constructed using compliance crack lengths continuously rise, while those constructed using the EPD crack lengths continuously fall. The rising form of the *R*-curve is typical for toughened ceramics, and several studies have reported similar *R*-curves using chevron and straight-through notched bend-specimens with compliance techniques on various ceramics and ceramic composites [5, 6, 20]. The falling *R*-curve is non-typical for this class of materials. Materials with falling (or flat) *R*-curve behavior should show unstable crack propagation, i.e., the material should be extremely brittle and should fail catastrophically but the fracture surfaces (Fig. 9) and the load-displacement plots (Fig. 6) do not exhibit such brittle characteristics.

Assuming that the compliance technique provides accurate *R*-curves, the differences in the *R*-curves of the composites can be correlated with their microstructures: weak fibre/matrix interaction in P100 results in huge crack branching and bridging that gives higher resistance to fracture, and so a rising *R*-curve behavior; the strong fibre/matrix bonding facilitates the crack growth by cutting through fibres, and thus shows only a very gently rising *R*-curve behavior. The *R*-curve behavior of both refractories are about the same, except

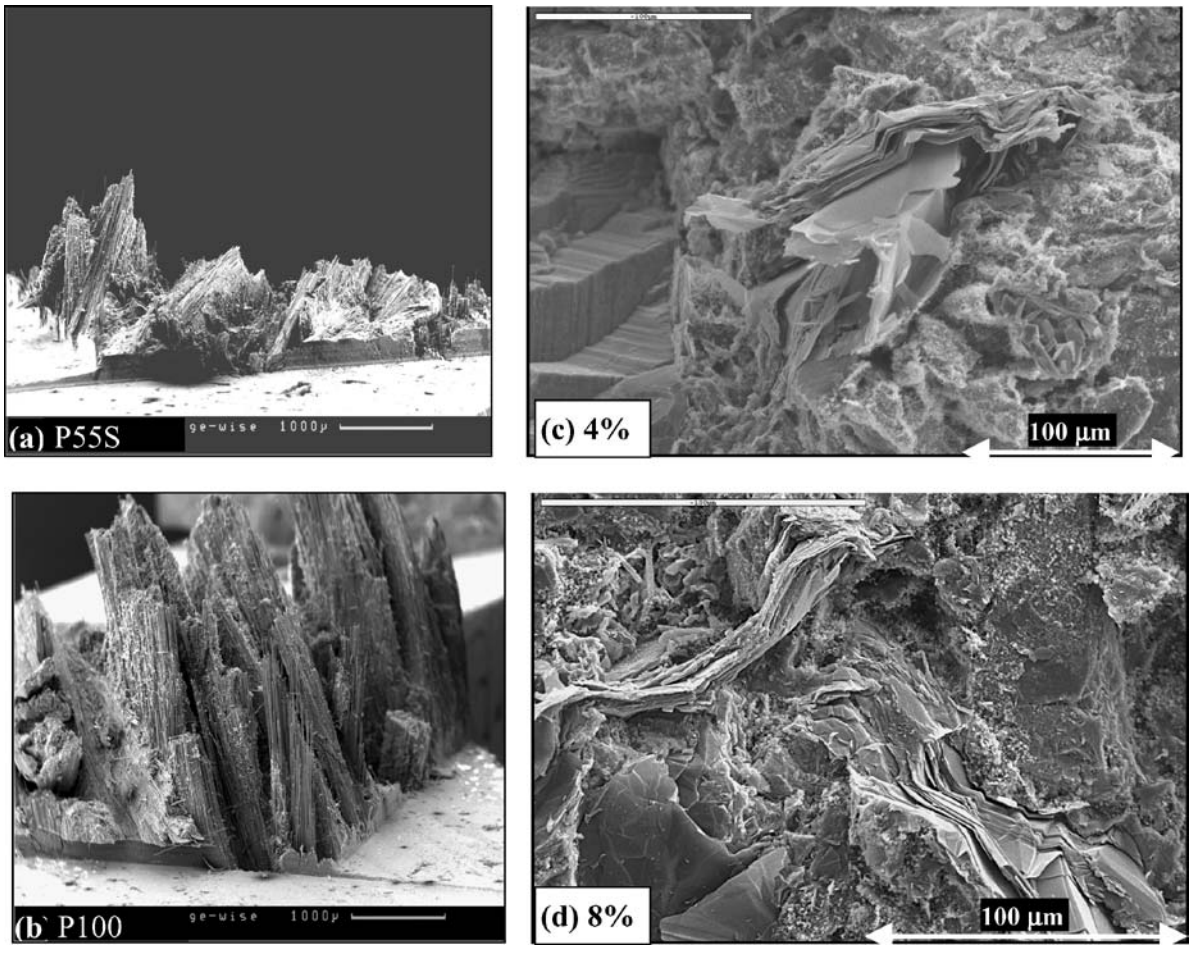

Figure 9 SEM images of fracture surfaces (one half) of the composites and refractories showing the extent of pull out of fibre/grains from the notch plane: (a) P55 S little pull out, (b) P100 huge pull out, (c) 4%, and (d) 8% both of which are nearly flat compared to composites.

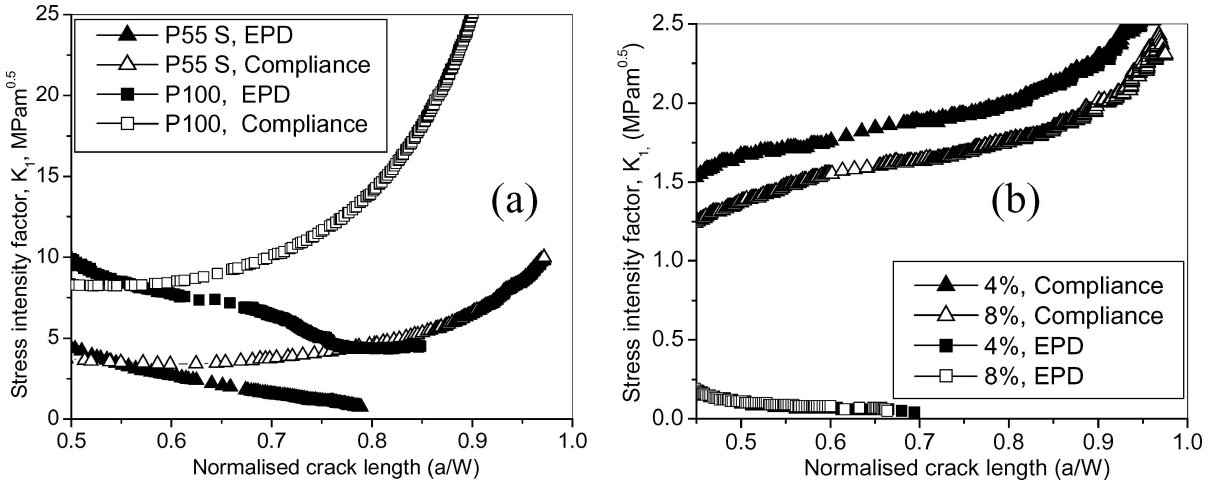

Figure 10 *R*-curves: (a) C/C composites and (b) carbon bonded refractories.

that the one with 4% graphite shows slightly higher K_1 values for any measured crack length. A higher flexural strength, flexural modulus and higher load carrying capacity during fracture testing for this refractory sample, Fig. 6, demonstrated its superiority over the refractory with 8% graphite.

3.4. Compliance versus EPD techniques as applied to composites and refractories

The compliance technique is based on the sample stiffness, which will depend on the mechanical link across the crack plane. The EPD technique is based on the continuity of the conduction path and the resistivity. Any surface contact across the crack plane would have an effect on the measured electrical resistance of the sample and result in an apparently shorter crack length than the real one. On the other hand, any sub-critical microcracking prior to the generation of a major crack would lead to an apparently longer crack length. Thus, the fracture characteristics of the materials are important in measuring crack length by both techniques. Defining the crack front in composite materials is difficult

as they create significant process zones, the damaged region just ahead and just behind the crack tip [19]. The zone size will depend on the microstructure of the composite. The zone is bigger in the P100 composite due to the weaker fibre/matrix interactions that allow fibre/matrix debonding and crack branching. There can be significant sub-critical cracking in the matrix prior to fracture taking place. The bridging fibres or grains in the process zone, as the crack continues to grow, will have different effects on the crack length measured by the different techniques. For the compliance technique, the stress carried by the bridging fibres or grains, the bridging stress, is important, but for the EPD technique what matters is just the physical contact between the constituents across the surfaces of the crack. As a result, for the same specimen under the same testing condition, the EPD and compliance techniques resolve different crack lengths. The EPD technique results in a large underestimation of crack length in the fracture region which is of interest for *R*-curve measurement. The discrepancy arises from the difference between the conditions of calibration and the actual fracture itself during mechanical testing. The calibration involves a clean cut across the notch plane (Fig. 5), but the mechanical testing produces process zones around the crack tip, around the notch plane (Fig. 9). The bridging of the crack in the wake by fibres or by carbon-coated alumina grains and graphite flakes in the refractory reduces the resistivity as compared to a "clean" crack. Thus, for materials of this type the crack lengths, once this zone is established, become significantly underestimated and should not be used to establish *R*-curves. Nevertheless, important information is given by the difference between the two crack length measurements which is related to the extent and nature of the bridging zone. In continuing work in this field we are examining this concept as an approach to gathering a better understanding of the toughening mechanisms of such materials.

4. Conclusions

1. Optical microscopy is not a desirable technique to measure the crack length in materials that develop large process zones, where the crack front is difficult to define. The technique is difficult to apply to chevron notched samples.

2. Even though the EPD technique has been used widely, crack bridging by conducting fibres or grains can cause underestimation of crack length in materials with significant bridging zones, due to the remaining electrical contact across the crack planes. Sub-critical cracking in composites can cause overestimation of crack length. *R*-curves that are constructed without accounting for such underestimation or overestimation are less meaningful.

3. A continuing comprehensive analysis of the refractories on the difference between the normalised crack lengths from the EPD and compliance techniques shows that it can give information about the extent of the bridging zone.

4. The C/C composite with the weaker fibre/matrix interface showed a significantly more steeply rising *R*-curve than the C/C composite with the stronger fibre/matrix interface and of the two refractories. The refractory with the lower graphite content showed higher stress intensity factors at all crack lengths, although their *R*-curves were similar in shape.

Acknowledgments

VPSR and SBF acknowledge financial support from Magnesita. S.A. (Brazil) and ESKOM/PBMR Co. (South Africa) respectively. The model refractory materials were kindly supplied by Magnesita S.A.

References

1. K. AHLBORN, T. CHOU, Y. KAGAWA and A. OKURA, *Carbon* **31** (1993) 205.
2. T. MIYAJIMA and M. SAKAI, *J. Mater. Res.* **6** (1991) 2312.
3. Y. L. WANG, U. ANANDAKUMAR and R. N. SINGH, *J. Amer. Ceram. Soc.* **83** (2000) 1207.
4. D. MUNZ, R. T. BUBSEY and J. L. SHANNON, *ibid.* **63** (1980) 300.
5. S. SENET, R. E. GRIMES, D. L. HUNN and K. W. WHITE, *Carbon* **29** (1991) 1039.
6. A. C. MAZZEI, J. A. RODRIGUES and V. C. PANDOLFELLI, *J. Mater. Sci.* **35** (2000) 2807.
7. R. A. RITCHIE and K. J. BATHE, *Int. J. Fracture* **15** (1979) 47.
8. K. H. SCHWALBE and D. HELLMANN, *J. Test. Eval.* **9** (1981) 218.
9. T. B. TROCZYNSKI and P. S. NICHOLSON, *Amer. Ceram. Soc. Bull.* **64** (1985) 1272.
10. N. MOTO, H. YANAGIDA, M. MIYAYAMA, T. NAKATSUJI, M. SUGITA and Y. OHTSUKA, *J. Ceram. Soc. Jpn.* **100** (1992) 585.
11. ASTM E647-96, "Annual Book of ASTM Standards" (West Conshohocken, Pennsylvania, USA, 1998).
12. R. H. DAUSKARDT, D. B. MARSHALL and R. O. RITCHIE, *J. Amer. Ceram. Soc.* **73** (1990) 893.
13. T. V. DUGGAN and M. W. PROCTOR, in "The Measurement of Crack Length and Shape During Fracture and Fatigue," edited by C. J. Beevers (Chameleon Press Ltd., London, 1980) p. 1.
14. H. SHIKANO, F. HATAKEDA, T. HONDA, T. ISCKI, H. NISHIDA, T. OKAMOTO, K. SAWANO, T. WATANABE and T. YANAGISAWA, in "Refractories Handbook" edited by Y. Takamiya, Y. Endo and S. Hosokawa (Technical Association of Refractories, Japan, Tokyo, 1997).
15. A. H. M. ANDREASEN and J. Z. ANDERSON, *Kolloid* **50** (1930) 217.
16. W. VIEIRA, JR., "Microstructure Development in Al_2O_3-C-Si Refractory Composites," PhD thesis, University of Leeds, UK, 1995.
17. ASTM C1421-99, "Annual Book of ASTM Standards" (West Conshohocken, Pennsylvania, USA, 1998).
18. H. L. EWALD and R. J. H. Wanhill, in "Fracture Mechanics" (Delftse Uitgevers Maatschappij b.v., The Netherlands, 1984).
19. B. McENANEY and T. MAYS, in "Essentials of Carbon-Carbon Composites," edited by C. R. Thomas (Royal Society of Chemistry, Cambridge, 1993) p. 143.
20. R. E. GRIMES, G. P. KELKAR, L. GUAZZONE and K. W. WHITE, *J. Amer. Ceram. Soc.* **73** (1990) 1399.

Received 21 August 2003
and accepted 18 May 2004